ORIGINAL ARTICLE

Microbial Complexes in Subgingival Plaque: A Bacterial Meta-Taxonomic Study

Julien Santi-Rocca[1] | David F. Martín-García[1] | Iván Lorca-Alonso[2] | Sandra la González-de la Fuente[2] | Begoña Aguado[2] | Mark Bonner[3] | Véronique Amard[4] | Pierre Amiot[4] | Charlotte Bar[4] | Vincent Berbon[4] | Nefissa Berkani[4] | Alix Burke[4] | Ivonne Cartagena[4] | Jean-Michel Chatard[4] | Céline Coutayar[4] | Guillaume Depraz[4] | Isabel Morales[4] | Narcisa Popa[4] | Stéphane Regniers[4] | Thomas Rissoan[4] | Catherine Robert[4] | Arnaud Tremoureux[4] | Marion Verdy[4] | Manuel Fresno Escudero[5,6,7] | Núria Gironès Pujol[5,6,7]

[1]Science and Healthcare for Oral Welfare, Toulouse, France | [2]Biocomputational Analysis Core Facility (SABio), Centro de Biología Molecular Severo Ochoa, Consejo Superior de Investigaciones Científicas, Universidad Autónoma de Madrid, Madrid, Spain | [3]International Institute of Periodontology, Victoriaville, Québec, Canada | [4]Association Médicale Contre les Infections Buccales (AMIB), Saint-Maur-des-Fossés, France | [5]Centro de Biología Molecular Severo Ochoa, Consejo Superior de Investigaciones Científicas, Universidad Autónoma de Madrid, Madrid, Spain | [6]Instituto de Investigación Sanitaria del Hospital Universitario de La Princesa, Madrid, Spain | [7]Departamento de Biología Molecular, Universidad Autónoma de Madrid, Madrid, Spain

Correspondence: Julien Santi-Rocca (jsr@periodontitis.show)

ABSTRACT

Aim: To leverage technological advances to propose a more accurate representation of subgingival microbiota diversity and dynamics across health and disease, 25 years after the seminal and still authoritative contribution of Socransky and his colleagues.

Materials and Methods: Subgingival plaque from 135 patients (41 healthy, 47 gingivitis, 47 periodontitis) was analysed by V3–V4 16S rRNA sequencing. Sequences were probabilistically assigned to unambiguous taxon groups (UTGs) using advanced bioinformatics. Beyond univariate analyses across health groups, samples were re-classified into microbiota patterns using unsupervised clustering. Bacterial community ordination was performed via correlation analysis.

Results: In total, 394 fully characterized UTGs were detected with a confidence level of at least 98% in all samples, with an average of 157 in each sample and 162 representing more than 95% of the bacteriome. Hierarchical clustering identified 10 UTG complexes, with 1 particularly associated with health (Complex 6) and 1 with disease (Complex 10). Complex 10 corresponded to 29 taxa, among which the three species from Socransky's red complex and additional 8 *Treponema* UTGs, as well as species from the orange complex. Complex 6 comprised species from Socransky's green, yellow and purple complexes. While gingivitis appeared as an intermediate state between health and periodontitis, k-clustering revealed five microbiota patterns related to disease progression, and with specific contributions of bacterial complexes, evidencing alternative pathophysiological routes.

Conclusion: These 10 new complexes offer an entry point to understanding plaque ecology, beyond the complexity of microbial dynamics in the periodontal microenvironments revealed by the variability within these groups and the existence of 'boundary taxa' linking them. These microbial complexes co-exist in specific microenvironments, and shifts in their relative abundance mark the transition from a healthy microbiota to a diseased microbiota, with intermediary patterns in between. We propose to

---

use these patterns as indicators for the classification of periodontal diseases along a microbial risk scale to complement the current staging and grading system.

1 | Introduction

Despite decades of research aimed at identifying periodontal pathogens, the exact composition and interactions within subgingival microbial communities remain only partially understood. Traditional identification methods, including early generation molecular techniques, have struggled to capture the full spectrum of involved bacteria and their intricate relationships.

Seminal studies, such as the landmark contribution of Socransky and his collaborators (Socransky et al. 1998), laid the groundwork by identifying key microbial complexes associated with periodontal health and disease. However, these studies were limited by the technology of their time, particularly in species targeting through hybridization and the low-resolution taxonomic assignment. While their identification of five bacterial complexes comprising 32 bacterial taxa advanced our understanding of periodontitis pathophysiology, our knowledge of the bacterial communities and their role in disease progression might still be incomplete or partially misrepresented.

High-throughput sequencing technologies, particularly metataxonomics using 16S rRNA gene sequencing, have revolutionized microbial community studies by offering an unprecedented resolution for taxon profiling in complex environments. When compared to DNA–DNA hybridization, next-generation sequencing prevents biases such as cross-reactivity of probes produced by random amplification of genomes. However, some bioinformatic challenges, such as taxon assignment errors when sequences match multiple taxa, persist (Fong et al. 2022). This often results in taxonomic assignments at higher ranks, usually at the genus level (Meuric et al. 2017; Jiao et al. 2022), which oversimplifies the data and reduces the hierarchical resolution. Despite estimates suggesting 774 (Escapa et al. 2018) to 1073 (Jiao et al. 2022) bacterial species in the human mouth, the number of assigned taxa remains lower, leading to potential mis-characterization of microbial diversity.

In this study, we hypothesize that periodontal health and disease are characterized by overlapping bacterial communities in varying proportions, reflecting distinct microenvironments within the subgingival niche. By applying a novel species assignment methodology, we aim to overcome the limitations of traditional bioinformatics and to provide a more accurate representation of microbial diversity. This research celebrates the *Journal of Clinical Periodontology*'s 50th anniversary and honours Socransky's legacy after 25 years by offering new insights into species clustering and into the ecological shifts leading to periodontitis, while re-introducing more clearly gingivitis in the frame. Our goal is to redefine with current technologies these microbial communities and their interactions, leading to the identification of new biomarkers and therapeutic targets involved in the transition from eubiosis and health to dysbiosis and periodontal diseases.

2 | Materials and Methods

2.1 | Study Population

A total of 135 patients (30–50 years old) from seven French clinics were recruited and divided into to three health categories: health, gingivitis and periodontitis. According to the EFP/AAP classification, the latter category corresponded to Stage II-III Grade B periodontal disease. All health practitioners underwent specific training to ensure the homogeneity of methods between clinics. More details are available in Materials and Methods of Supporting Information.

2.2 | Sample Collection and DNA Purification

Subgingival plaque was sampled with a periodontal probe from the deepest site and conserved in 50 μL of TEGI medium as previously described (Bonner et al. 2014), kept at 4°C during the collection time at the dental clinic and then sent to UAM in batches, where they were kept at −80°C. After dilution of the sample with 300 μL water, DNA purification was performed using the MagMax Viral/Pathogen Ultra Nucleic Acid Isolation kit (Applied Biosystems). More details are available in Materials and Methods of Supporting Information.

2.3 | Bacterial Meta-Taxonomic Sequencing

Purified DNA was quantified and amplified for Illumina sequencing using 341F and 806R primers for the first amplification of the V3–V4 regions of 16S rRNA gene (Klindworth et al. 2013). The technical specifications and all steps prior to sequencing in a 2 × 300 pair-end sequencing run on a MiSeq sequencer are described in Materials and Methods of Supporting Information.

2.4 | Taxonomic Classification

Sequence classification was performed using BLAST within QIIME2 against the extended Human Oral Microbiome (eHOMD) database (Escapa et al. 2020). A threshold of 98% minimum sequence identity and query coverage was used to retrieve up to a limit of 500 hits per featured ID (FID). Subsequently, a first consensus-based taxonomic assignment was carried out within QIIME2 with default parameters.

Then, in order to further identify other possible non-canonical oral species, the FIDs remaining unassigned were queried against the 16S RefSeq Targeted Loci Project Archaea and Bacteria database (https://www.ncbi.nlm.nih.gov/refseq/targetedloci/) with the same BLAST parameters.

Lastly, to overcome the common problems of low taxonomic rank and exclusion of closely related matches (or even ex aequo results),

we have developed a 'probabilistic and non-exclusive' (PRONEX) method for taxonomic assignment. The methodology is described in detail in Materials and Methods of Supporting Information, and the script used in R is available at GitHub (https://github.com/JSR-SHOW/SHOW_4_The_World/blob/82fd41ffccef5a0b1ba665d8deb99abb28808e7b/PRONEX). This method is applied to the combined database searches and compared with the powerful and widely used QIIME2 tool (Figure S1).

2.5 | Hierarchical Clustering

The oligodendrogram was produced in R. The correlation matrix between species was computed using Pearson's correlation coefficient. Hierarchical clustering was then performed using the complete linkage method. The complete script is available in Materials and Methods of Supporting Information.

2.6 | Correlation Network Analysis

Network associations between UTGs were analysed in R. An undirected, weighted graph was created using the Pearson's correlation matrix, with nodes sized by mean abundance and coloured by predefined group colours. The complete script is available in Materials and Methods of Supporting Information.

2.7 | Microbiota Pattern Discrimination

The microbiota patterns were analysed in R. Patients were grouped using k-means clustering to reflect the composition of their microbiota. The complete script is available in Materials and Methods of Supporting Information.

2.8 | Statistical Analysis

Most graphs and analyses were produced with GraphPad Prism 8, with prior data preparation in Excel. Means were compared using Student's *t*-test for homoscedastic groups or Welch's *t*-test for heteroscedastic groups, based on the results of Fisher's *F*-test.

2.9 | Ethics

This study was approved by the UAM Ethics Committee (CEI-101-1907). Patients were informed of their rights regarding the use of their samples, personal information and the data generated, in accordance with national and European regulations.

3 | Results

3.1 | Diversity of Bacterial Taxa in Health and Disease

After filtering out low-abundance FIDs, a total of 588 taxa were identified, which were grouped into 394 unambiguous taxon groups (UTGs, detailed in Tables S1–S3) using our PRONEX method and ordered according to decreasing mean abundance in all samples. The majority of these UTGs were constituted of a single taxon (315, 79.9%), 42 of two taxa (10.7%) and 22 of three taxa (5.6%), as presented in Figure S1. Almost all UTGs were assigned at the species or subspecies level, 97.9% of reads, as compared to 44.8% for the classical QIIME2 method (Figure S2), and approximately 40% of the listed taxa (239 out of 588) represented uncultured phylotypes. In each sample, a mean of 157 UTGs was detected, with 142 UTGs more abundant than 1 UTG read for 10^4 total reads, 81 UTGs more abundant than 1 for 10^3 and 22 UTGs more than 1 for 10^2 (Figure 1A). The disease state had an impact on microbiota diversity, as evidenced by an increasing alpha diversity along disease severeness (Figure 1B). In parallel, the average number of UTGs needed to represent 50% of the reads was 5.38 (95% CI: 5.36–5.39) in health, 7.60 (95% CI: 7.58–7.63) in gingivitis, 9.19 (95% CI: 9.16–9.12) in periodontitis and 7.35 (95% CI: 7.20–7.50) in all conditions (Figure 1C,D).

For better readability in statistical analyses, we selected 162 UTGs of interest—the most abundant ones, covering 95% of the reads in all samples.

3.2 | Associations Among Bacterial UTGs as Determined by Cluster Analysis

We performed an association analysis and hierarchical clustering using the complete linkage method to classify UTGs according to the covariance of their abundance in samples.

The 135 samples and the selected 162 UTGs were used to cluster the latter in bacterial complexes. The number of complexes was fixed to 10 (Figure 2) and corresponded to the optimal level of details for the subsequent analyses. Complex 2 had the least number of UTGs, 7, while Complex 10 had the highest number of UTGs, 29.

Some classical markers of health, namely *Streptococcus gordonii* (UTG003), *Veillonella parvula* (UTG005), *Streptococcus sanguinis* (UTG027), and *Capnocytophaga sputigena* (UTG071), were grouped in Complex 6 together with 14 other UTGs. Among them, *Actinomyces* sp. HMT 170/*Actinomyces viscosus* (UTG090) was occasionally associated by Socransky to the health-associated 'purple complex' comprising *V. parvula* (Socransky et al. 1998). Traditional markers of disease, namely *Porphyromonas gingivalis* (UTG007), *Tannerella forsythia* (UTG025), and *Treponema denticola* (UTG028), Socransky's red complex, were grouped in Complex 10 together with 8 other *Treponema* UTGs, 3 *Prevotella* UTGs, 3 *Fretibacterium* UTGs, *Porphyromonas endodontalis* (UTG017), *Campylobacter rectus* (UTG020), and 10 other UTGs.

Species of the *Treponema* genus, with their corkscrew-shaped body characteristic of spirochaetes, as well as the vibrio-like and the rather abundant *C. rectus*, exhibit high motility, which contrast with the members of Complex 6 that are mostly sessile: cocci (*S. gordonii* [UTG003], *V. parvula* [UTG005], *Neisseria mucosa* [UTG015], *S. sanguinis* [UTG027], *Granulicatella adiacens* [UTG068] or *Abiotrophia defectiva* [*UTG106*]), rod-shaped bacilli (*Haemophilus parainfluenzae* [UTG012], *Lautropia mirabilis* [UTG018], *Prevotella*
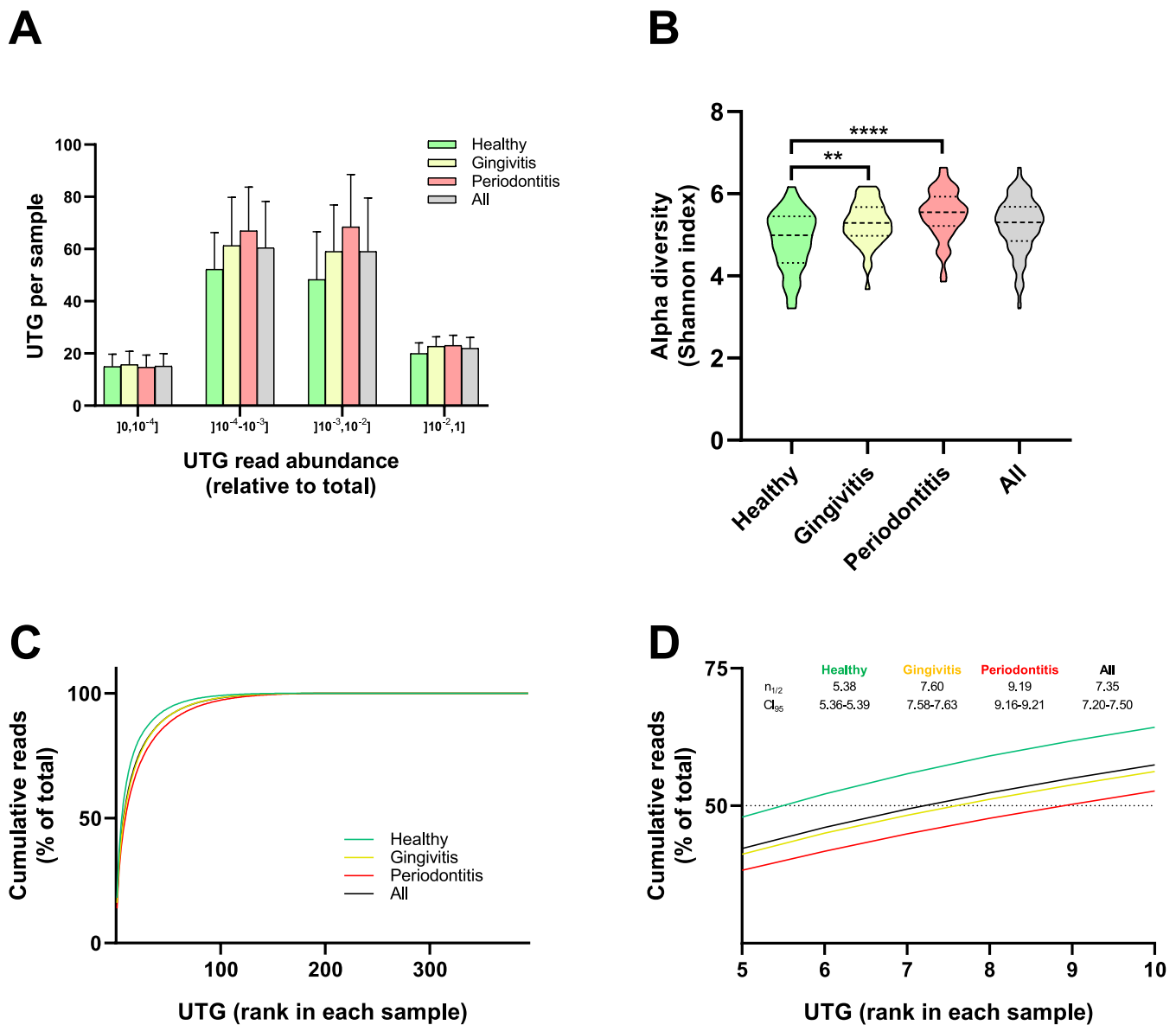
FIGURE 1 | Unambiguous taxon group richness in plaque samples. Scattering of UTG in samples was evaluated by the relative abundance of their assigned reads in samples (Panel A), by alpha diversity, as measured by Shannon index (Panel B), and by the cumulative read abundance according to the UTG rank in each sample (Panel C, zoomed in, Panel D). In Panel B, mean alpha diversity was significantly higher in gingivitis and in periodontitis as compared to healthy individuals ($p = 2.7 \times 10^{-3}$ and $p < 10^{-4}$, respectively, using Student's/Welsh's t-test). The difference of the means observed between gingivitis and periodontitis groups was not significant ($p = 5.7 \times 10^{-2}$).

melaninogenica [UTG040], *Kingella oralis* [UTG042], *Riemerella* sp. HMT 322 [UTG063], *Haemophilus pittmaniae* [UTG070] or *Neisseria bacilliformis* [UTG081]), fusiform bacilli (*C. sputigena* [UTG071]) and filaments (*A.* sp. HMT 170 [UTG090] or *Actinomyces oris* [UTG150]).

3.3 | Bacterial Taxa as Individual Markers of Health and Disease

The abundance of UTGs in samples is detailed in Table S4 and analysed according to clinically diagnosed health status in Tables S5 and S6, with a comprehensive representation in Figure 3.

The abundance of a large number of UTGs was modulated between health and disease (46 relatively more abundant in disease, 13 in health; Figure 3D), particularly between periodontitis and health (45 more abundant in periodontitis, 19 in health; Figure 3B) or between gingivitis and health (38 in gingivitis, 11 more abundant in health; Figure 3A). The bona fide markers of disease, namely *P. gingivalis* (UTG007, Complex 10), *T. forsythia* (UTG025, C10) and *T. denticola* (UTG028, C10), were more abundant in all disease conditions compared to health. Other Treponema UTGs were more abundant in periodontitis compared to health: *T. socranskii* (UTG024, C7), *T.* sp. HMT 237 (UTG032, C10), *T. medium* (UTG047, C8), *T. maltophilum* (UTG083, C10), *T. lecithinolyticum* (UTG117, C10), *T.* sp. HMT 253 (UTG123, C10), *T.* sp. HMT 257 (UTG130, C10), *T.* sp. HMT

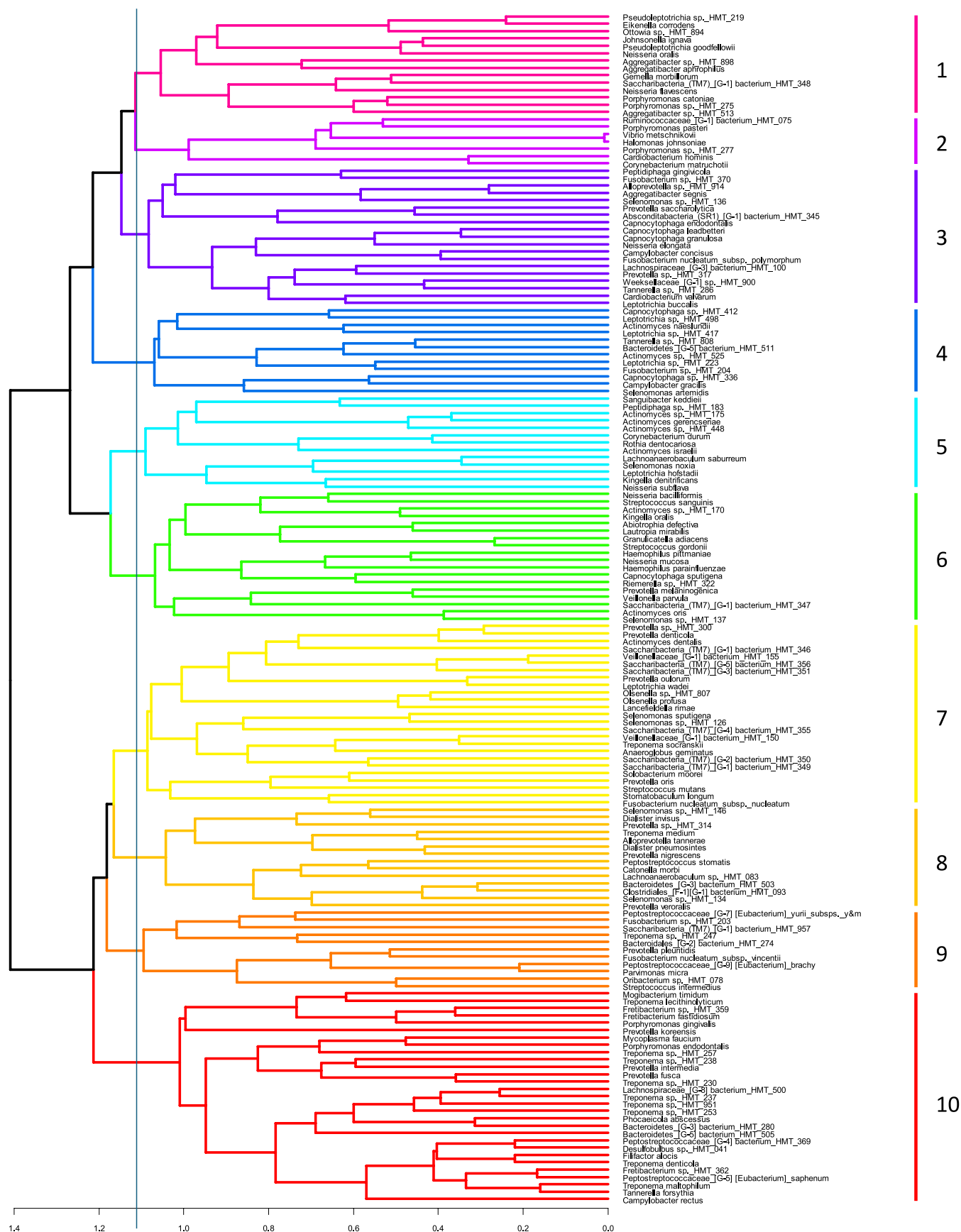**FIGURE 2** | Hierarchical clustering of UTGs into complexes. Correlation analysis was performed using all samples. Ten complexes were chosen based on the number of UTGs by group, revealing the proximity to the closest neighbour. The distance was calculated as $1 - R_{Pearson}$, ranging from 0 for perfect positive correlation to 2 for perfect negative correlation. The vertical line represents the cutoff for 10 complexes.
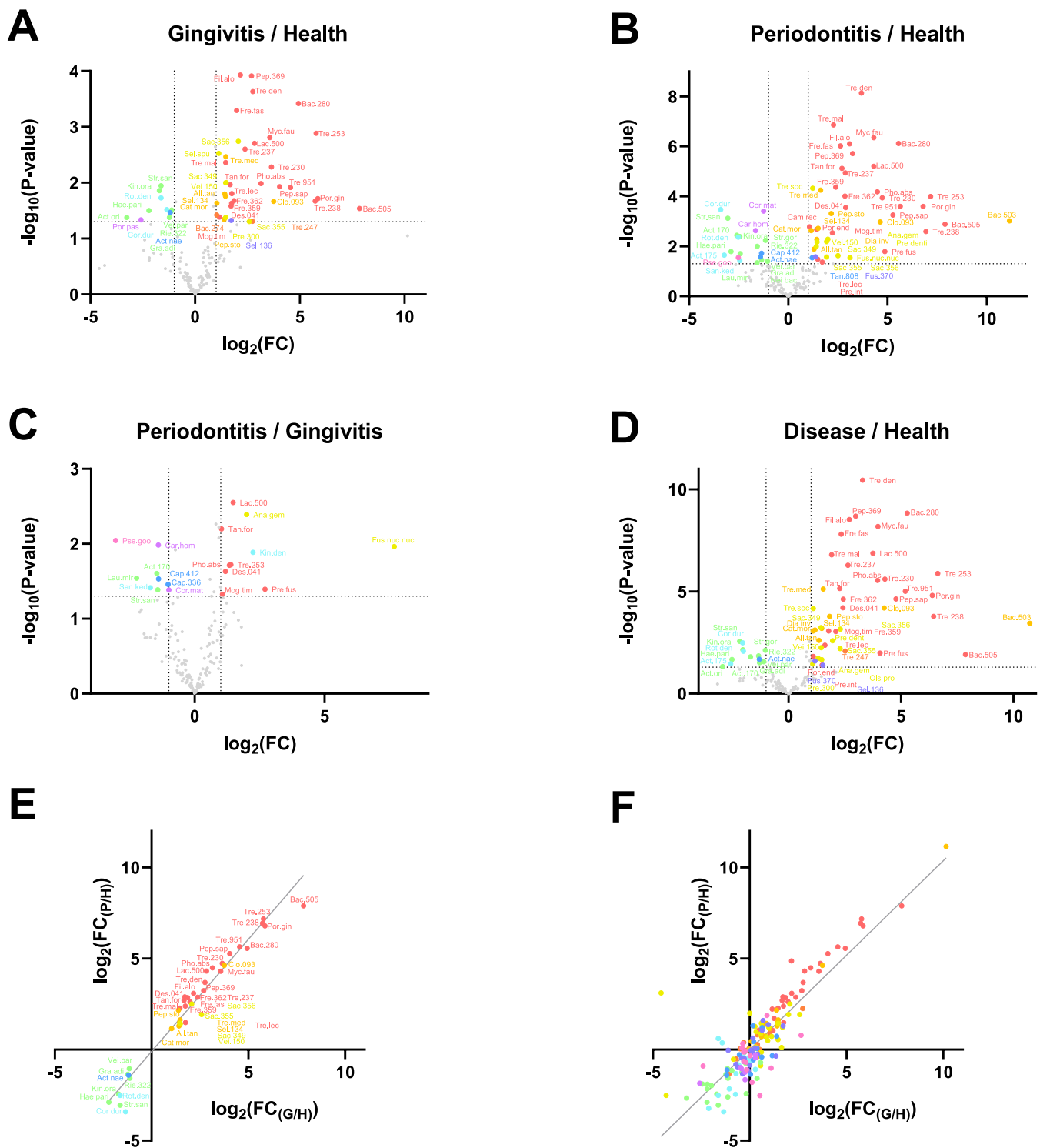
FIGURE 3 | Legend on next page.

247 (UTG133, C9) *T.* sp. HMT 238 (UTG135, C10), *T.* sp. HMT 230 (UTG137, C10) and *T.* sp. HMT 951 (UTG160, C10).

Some other UTGs are always more abundant in health: *V. parvula* (UTG005, C6), *Rothia dentocariosa* (UTG010, C5), *H. parainfluenzae* (UTG012, C6), *S. sanguinis* (UTG027, C6), *K. oralis* (UTG042, C6), *R.* sp. HMT 322 (UTG063, C6), *G. adiacens* (UTG068, C6), *Corynebacterium durum* (UTG075, C5) and *Actinomyces naeslundii* (UTG127, C4).

Comparing gingivitis and periodontitis, the number of UTGs with relative overabundance is modest (10 more abundant in periodontitis, 9 more abundant in gingivitis; Figure 3C). UTGs of interest in Panels A and B are 2.234 more abundantly modulated in periodontitis versus gingivitis ($R^2 = 0.967$; Figure 3E, $\log_2$ scale); this result is confirmed using the 162 UTGs, albeit with less confidence (slope = 2.009, $R^2 = 0.999$; Figure 3F, $\log_2$ scale). Noteworthily, *Pseudoleptotrichia goodfellowii* (UTG152, C1) and *Fusobacterium nucleatum* subsp. *nucleatum* (UTG093,

FIGURE 3 | Relative abundance of UTGs between conditions. The volcano plots (Panels A–D) show the p-value ($-\log_{10}$) corresponding to the fold change ($\log_2$) for each UTG. The UTGs of interest (solid circles, with representative species name) were determined by a significant ($p < 0.05$, above the horizontal dashed line) and substantial (FC ≥ 2 or FC ≤ 0.5, outside the vertical dashed lines) variation in abundance between the two compared conditions: gingivitis versus health (Panel A), periodontitis versus health (Panel B), periodontitis versus gingivitis (Panel C), disease (pooled gingivitis and periodontitis) versus health (Panel D). The rest of the first 162 UTGs were represented as grey points. For instance, as shown in Panel B, *Porphyromonas gingivalis* is 110.49 (6.79 in $\log_2$ scale) more abundant in periodontitis samples as compared to healthy ones, and this difference is significant ($p = 2.56 \times 10^{-4}$, 3.59 in ($-\log_{10}$) scale). Comparison of relative abundance of the UTGs of interest in Panels A and B (Panel E), and of the 162 first UTGs (Panel F). UTGs are plotted according to their FC ($\log_2$ scale) between gingivitis and health (x-axis) against their FC ($\log_2$ scale) between periodontitis and health (y-axis). The changes in abundance for the UTGs of interest are linear ($\log_2$ scale: $R^2 = 0.960$, slope $= 1.230$, Panel E; linear scale (excluding the outlier Bacteroidetes [G-5] bacterium HMT 505, UTG122): $R^2 = 0.967$, slope $= 2.234$, individual data not presented as a graph but available in Table S5), whereas the linear correlation is not as strong for the first 162 UTGs ($\log_2$ scale: $R^2 = 0.763$, slope $= 1.039$, Panel F; linear scale (same UTG excluded): $R^2 = 0.999$, slope $= 2.009$, individual data not presented as a graph but available in Table S5). The colours of the solid circles correspond to those of the classification of complexes in Figure 2.

C7) exhibited the highest fold changes between gingivitis and periodontitis—positive and negative—respectively, but their low prevalence—66 and 121 negative samples, respectively—calls for caution about their relevance in distinguishing the two health states.

Considering the mean abundance in each complex as represented in Table S6, Complex 6 demonstrates a clear association with health, being 2.48 (0.403^{-1}) times more abundant in healthy samples as compared to those with disease. Similarly, Complexes 5 and 2 are also associated with health, with relative abundance levels of 2.11 (0.475^{-1}) and 1.71 (0.586^{-1}), respectively. In contrast, Complex 10 is outstandingly correlated with disease, being on average 5.15 times more abundant in disease samples than in healthy ones. Additionally, Complexes 8 and 9 show a lesser yet significant association with disease, being 2.00 and 1.73 more abundant, respectively.

3.4 | Relationship Among UTGs

The relationship among UTGs in all samples, in terms of correlation intensity and strength of associations within microbiota, is illustrated in Figure 4. Each node represents a UTG, coloured by complex and sized by average abundance in samples, with link width reflecting the strength of dyadic correlations. Our analysis was compared to Socransky's study using corresponding UTGs, which showed their consistency (Figure S8).

UTGs are grouped in two hemispheres: health markers (top-right corner) and disease markers (bottom-left corner) mark the extremities of the network. Complex 7 (yellow) is central, and other few edges bridging 'boundary taxa' are visible, suggesting that different paths exist between the health and disease hemispheres.

Despite a clear tendency for bacteria within each complex to be grouped together as a result of dense intra-group relationships, these internal correlations within complexes compete with the—sometimes strong or multiple—dyadic correlations that certain bacteria exhibit with bacteria from other complexes. Typically, the UTGs of complexes that are extremely linked to disease—Complex 10, in red—or health—Complex 6, in green—are strongly grouped together in a zone of the graph

and exhibit strong dyadic correlations within their group, with only scarce individual correlations with UTGs of close external groups. In contrast, other intermediate groups whose UTGs are more dispersed in the graph show significant dyadic correlations with only a few other UTGs within their group and remarkable correlations with the UTGs of one or more other groups: this is typically the case for Complexes 9 (orange) and 4 (blue). Complex 9 seems to be a group of ecological connectors, like *Oribacterium* sp. HMT 078 (UTG102, C9) between the yellow (C7) and amber (C8) Complexes, or like the ubiquitous *F. nucleatum* subsp. *vincentii* (UTG001, C9), the more discrete *Prevotella pleuritidis* (UTG073, C9) and the species formerly known as *Eubacterium brachy* ("Pep.bra", UTG108, C9), connecting these same yellow and amber Complexes with bacteria of the red (C10) and blue (C4) Complexes. In the same vein, *Campylobacter gracilis* (UTG008, C4) appears as a boundary species between bacteria from the cyan (C5) and yellow (C7) Complexes. It is itself particularly well correlated with two UTGs from its own complex, *Capnocytophaga* sp. HMT 336 (UTG049, C4) and *Fusobacterium* sp. HMT 204 (UTG013, C4), which are otherwise poorly connected to each other while each of them connects very well with some UTGs from the pink (C1) and purple (C2) Complexes, for the former, and the orange Complex (C9) for the latter.

3.5 | Microbiota Patterns and Clinical Parameters

Clinical diagnosis of periodontal diseases reflects damages from infection, lagging behind microbiota shifts. We thus proposed to identify general microbiota patterns using k-clustering of samples based on the UTG abundance, comparing the obtained classes to clinical parameters. Five patterns ($k = 5$, Figure S3) classified samples clearly, as evidenced in 2D projections (Figure 5A,B) and 3D representations (Figures S4–S6). Interestingly, the best fit from the 'Silhouette' curve (Figure S3B) gives an optimal number of clusters, $k = 2$. This solution was explored (Figure S7) and led to a binary pattern scattering contrasting a rather healthy microbiota pattern with another clearly associated with disease and more specifically periodontitis. This classification was not used for later analysis but is still presented in Table S4.

Pattern D contains only 4 samples, while the others comprised between 23 and 43 (Figure 5C). The sequence of patterns (A–E,
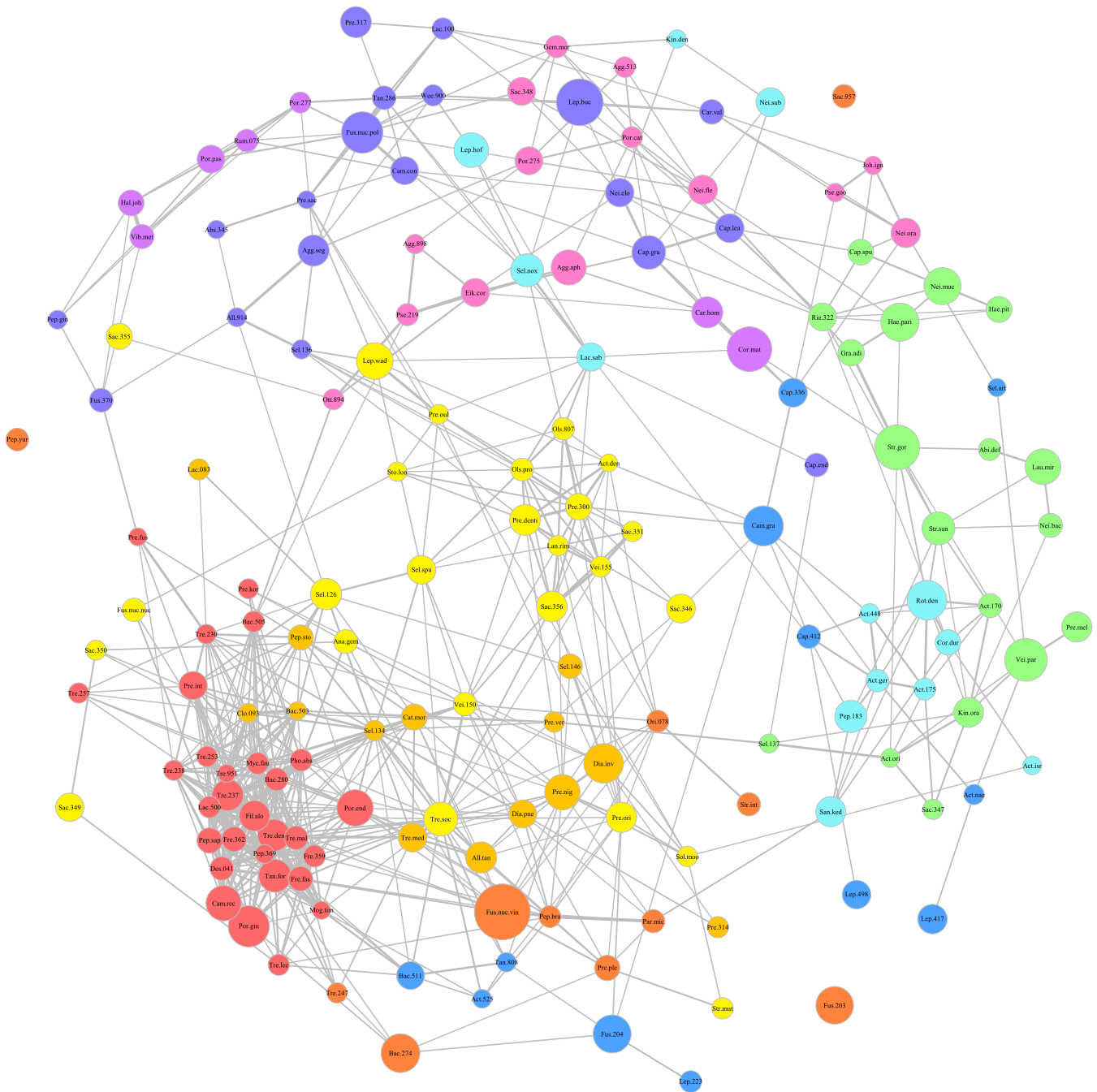
FIGURE 4 | Network graph of UTG correlations. The graph displays the correlations between UTGs based on Pearson correlation coefficients calculated from all samples. Nodes represent UTGs, and edges represent significant positive correlations (threshold ≥ 0.3). Edge width is proportional to the strength of the correlation. Node size reflects the mean abundance of each UTG, and node colour corresponds to predefined complex numbers from Figure 2: Complex 1 (pink), Complex 2 (purple), Complex 3 (lilac), Complex 4 (blue), Complex 5 (cyan), Complex 6 (green), Complex 7 (yellow), Complex 8 (amber), Complex 9 (orange), Complex 10 (red). It is noteworthy that this methodology was assayed using only targets from the Socransky's study, yielding consistent results with their conclusions and supporting their model in a different set-up (Figure S8).

in alphabetical order) unfolds a gradual progression towards a highest probability of periodontal disease, with gingivitis representing an intermediary stage. Alpha diversity, measured by the Shannon index, tends to increase along this sequence (Figure 5D) as it did with disease severity (Figure 1B), with the notable exception of Pattern D, yet poorly significant with only four samples.

Patterns' relevance is supported by the large number of modulated UTGs, consistent with the classification method (Figure 5E–I, details in Table S7). Furthermore, markers of health and disease (identified in Figure 3) align with this classification, suggesting the co-occurrence of some UTGs. Notably, *P. gingivalis* is more abundant only in Pattern E and down-regulated in all others while totally absent from
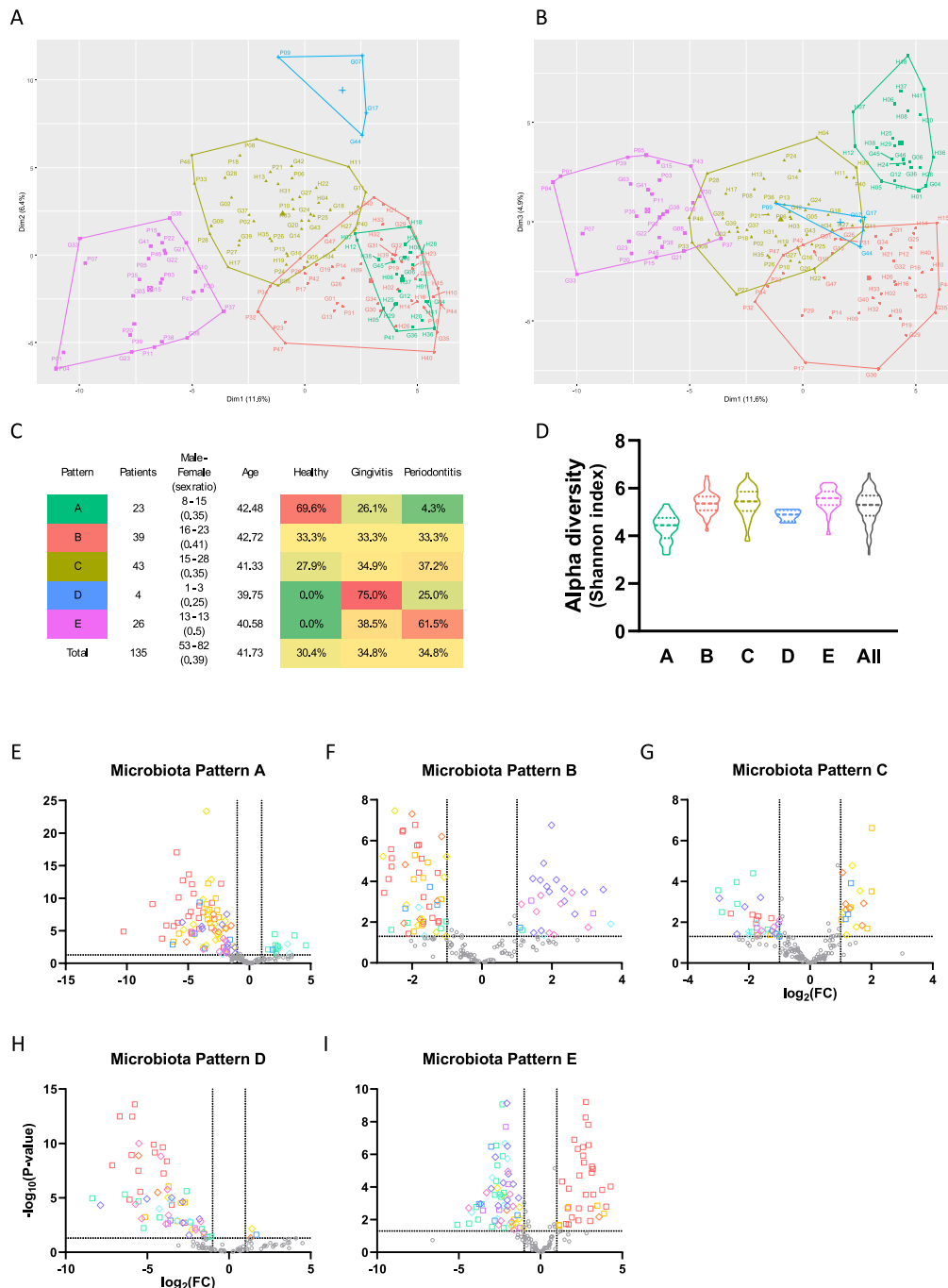
FIGURE 5 | Microbiota patterns. Classification of samples according to their bacterial content was performed by k-clustering. After determining the optimal number of clusters thanks to the elbow method ($k = 5$, Figure S7), individual samples were projected in a principal component space: Dimension 1 and Dimension 2 (Panel A), Dimension 1 and Dimension 3 (Panel B). Three-dimensional representations are presented in Figures S4–S6. Samples were labelled with their names, the first letter standing for the health state determined during clinical examination: 'H' for healthy, 'G' for gingivitis and 'P' for periodontitis (Table S4). Data about the patients for each of the 5 microbial patterns are presented in Panel C, namely the number of patients, the repartition between males and females, the mean age and the percentage of each health group contributing to the pattern. Alpha diversity for each microbial pattern is presented in Panel D and comparison for each group with the other ones were performed by Student's/ Welsh's *t*-test, which reveal all groups presented means significantly different from each other groups ($p < 5 \times 10^{-2}$), except B and C ($p = 0.742$), B and E ($p = 0.217$) and C and E ($p = 0.414$). For readability concerns, significance indicators were not presented on the plot. The volcano plots (Panels E–I) show the *p*-value ($-\log_{10}$) corresponding to the fold change ($\log_2$) for each UTG. The UTGs of interest (diamonds when belonging to complexes with odd numbers, squares for even-numbered complexes, with colours corresponding to those used in Figures 2 and 4) were determined by a significant ($p < 0.05$, above the horizontal dashed line) and substantial (FC ≥ 2 or FC ≤ 0.5, outside the vertical dashed lines) variation in abundance between the two compared groups: Microbial Pattern A–E (Panels E–I) versus the rest of the samples in each case. Other UTGs were represented as grey circles.

Pattern D, indicating another disease profile not based on *P. gingivalis* or painting it as a late assailant rather than an early contaminant.

3.6 | Relationship Between Bacterial Complexes and Clinical Parameters

To simplify microbiota visualization across patterns, we generated network graphs using complexes instead of individual UTGs (Figure 6). The scales in Figures 6 and S9 are identical with disc surfaces proportional to bacterial abundance in each complex. Figure S9A illustrates the relationship between UTG complexes in all the samples, showing a close-to-linear transition from highly modulated health markers (Complex 6, green) to highly modulated disease markers (Complex 10, red), through several possible ecological pathways: 6–5–4–9–10 or 6–5–4–7–8–10. Noteworthily, some longer or alternative paths include Complex 2, or Complexes 1 and 2, before connecting again with disease-associated complexes through Complex 4. Notably, Complex 4 remains nearly constant across all patterns, and acts mostly as a connector between health-associated complexes and disease-associated ones. Complex 3 appears as a satellite of Complex 1 and 2.

In this model, Pattern D stands aside, with a strong representation of Complex 7 and low abundance of the disease-associated Complexes 8, 9 and 10. This suggests that Complex 7, although initially identified as intermediate due to clinical diagnosis inference, may be an alternative endpoint with possible both-way switching with Complex 8, implying that Pattern D could reflect another type of periodontal disease not based on usual disease-linked bacterial complexes but notably associated with a drastic repression of the Pattern B-associated bacteria of Complex 1.

## 3.7 | Relationship Between UTGs and Patterns

The overall association strength of each UTG to its complex was evaluated by the mean correlation to other complex members, calculated by Pearson's *R* coefficient (Tables 1 and S8). As observed in Figure 6 and evidence by the low 'boundary index' in Table S8 (normalized ratio of the correlation with UTGs from other complexes and the correlation with the UTGs of its own complex), Complex 10 UTGs appear to form a sturdy complex. The high mean coefficient of variation for Complex 10 shows a noticeable variation of abundance of its UTGs between patterns, all being more abundant in Pattern E. Conversely, Complex 4 showed a high boundary index and a low coefficient of variation, confirming its place in Figure 6 as a ubiquitous intermediary complex with an overall constant abundance. At the individual level, the most abundant UTG of Complex 4, namely *C. gracilis* (UTG008, C4), is more abundant in Pattern D and is linked to three UTGs of Complex 7, three of Complex 4 and of Complex 5 (Figure 4).

Lastly, Complex 6, associated with health (Pattern A), showed the second highest mean coefficient of variation, with all its UTGs having their highest abundance in Pattern A (except for *N. bacilliformis*, UTG081, C6, with a maximum abundance in
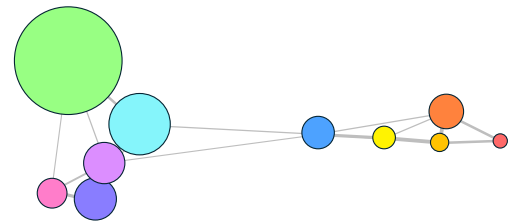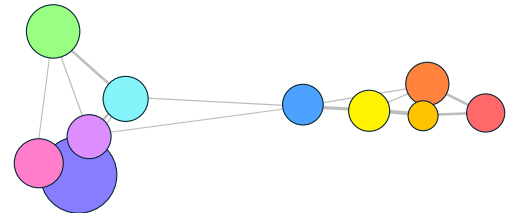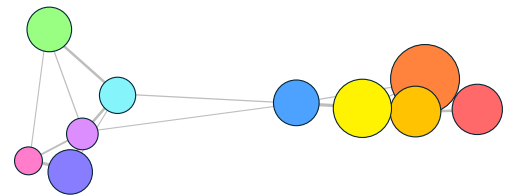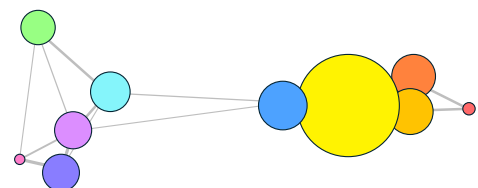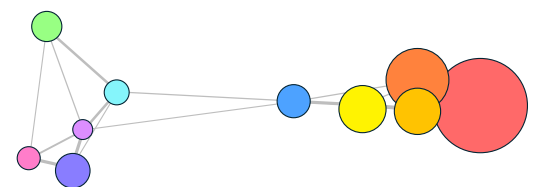
FIGURE 6 | Contribution of bacterial complexes to the microbiota patterns. Bacterial complex abundance was obtained by summing the abundance of all the UTGs they comprise. The graph displays the correlations between complexes based on Pearson correlation coefficients calculated for each indicated microbial pattern. Nodes represent bacterial complexes, their size is proportional to their abundance and edges represent significant positive correlations (threshold ≥ 0 for the template using all samples in Panel A, copied in the following panels). The interactions between complexes in other conditions are visible in Figure S8.

TABLE 1 | Contribution of UTGs to complexes and patterns.

Identification			Correlation			Abundance in patterns (relative to max)				
UTG	Repr. species	Complex	Within complex	With others	Maximum abundance	A	B	C	D	E
21	Agg.aph	1	0.185	−0.035	1.97E-02	47.7%	100.0%	54.5%	3.5%	36.0%
43	Nei.fle	1	0.155	−0.035	1.24E-02	67.5%	100.0%	16.9%	0.0%	9.6%
44	Nei.ora	1	0.188	−0.020	1.21E-02	57.4%	100.0%	34.1%	3.5%	2.9%
55	Eik.cor	1	0.259	−0.028	1.01E-02	32.1%	100.0%	30.3%	12.8%	34.5%
58	Por.275	1	0.255	−0.023	1.20E-02	12.3%	100.0%	21.8%	3.1%	14.6%
4	Cor.mat	2	0.208	−0.042	4.72E-02	100.0%	87.9%	58.1%	95.6%	18.2%
34	Car.hom	2	0.164	−0.026	1.36E-02	62.2%	100.0%	38.8%	19.7%	16.5%
64	Por.pas	2	0.300	−0.035	1.00E-02	68.6%	100.0%	19.8%	3.7%	5.1%
67	Hal.joh	2	0.393	−0.019	5.34E-03	88.9%	91.1%	51.2%	100.0%	43.2%
80	Vib.met	2	0.388	−0.020	4.16E-03	92.1%	86.9%	46.1%	100.0%	44.2%
2	Lep.buc	3	0.190	−0.035	6.95E-02	26.7%	100.0%	44.2%	39.1%	31.9%
6	Fus.nuc.pol	3	0.260	−0.048	5.05E-02	33.8%	100.0%	28.9%	13.7%	13.2%
23	Cap.gra	3	0.178	−0.050	2.11E-02	44.7%	100.0%	31.2%	22.1%	14.3%
31	Agg.seg	3	0.218	−0.031	1.89E-02	43.8%	100.0%	7.1%	0.2%	8.0%
33	Pre.317	3	0.164	−0.014	1.08E-02	22.0%	100.0%	87.0%	10.1%	46.6%
8	Cam.gra	4	0.212	−0.016	5.07E-02	35.0%	36.3%	52.6%	100.0%	22.5%
13	Fus.204	4	0.165	−0.011	2.82E-02	33.9%	43.7%	100.0%	44.7%	38.2%
41	Lep.417	4	0.081	−0.006	1.33E-02	4.3%	100.0%	38.0%	70.8%	7.8%
49	Cap.336	4	0.059	−0.013	9.87E-03	46.8%	91.0%	46.2%	100.0%	24.2%
52	Lep.498	4	0.079	−0.007	8.10E-03	1.0%	100.0%	82.1%	22.4%	54.6%
10	Rot.den	5	0.205	−0.059	7.39E-02	100.0%	9.6%	18.1%	10.2%	4.1%
22	Lep.hof	5	0.051	−0.026	2.30E-02	28.2%	100.0%	40.6%	23.5%	12.2%
26	Sel.nox	5	0.137	−0.018	2.34E-02	27.5%	60.8%	40.8%	100.0%	10.5%
29	Pep.183	5	0.109	−0.017	1.89E-02	100.0%	27.9%	38.9%	2.4%	41.2%
45	Nei.sub	5	0.013	−0.015	1.61E-02	8.6%	100.0%	11.4%	0.0%	2.3%
3	Str.gor	6	0.240	−0.100	8.94E-02	100.0%	27.3%	30.4%	17.3%	8.7%
5	Vei.par	6	0.174	−0.079	7.35E-02	100.0%	20.9%	35.1%	11.8%	8.6%
12	Hae.pari	6	0.209	−0.090	8.41E-02	100.0%	6.0%	3.8%	1.1%	2.1%
15	Nei.muc	6	0.194	−0.073	4.55E-02	100.0%	46.2%	5.8%	0.1%	5.8%
18	Lau.mir	6	0.194	−0.056	3.74E-02	100.0%	38.4%	9.1%	0.8%	21.2%
16	Lep.wad	7	0.135	−0.026	8.04E-02	3.8%	19.0%	25.2%	100.0%	4.3%
24	Tre.soc	7	0.222	0.020	1.65E-02	6.6%	36.8%	92.8%	97.4%	100.0%
30	Sel.126	7	0.075	0.039	1.05E-02	10.1%	91.4%	82.0%	24.4%	100.0%
35	Sac.356	7	0.295	−0.025	6.80E-02	0.3%	4.0%	14.2%	100.0%	9.5%
37	Pre.denti	7	0.271	−0.028	6.66E-02	1.9%	3.2%	18.0%	100.0%	6.0%
9	Dia.inv	8	0.192	−0.002	4.60E-02	8.1%	22.8%	72.5%	100.0%	46.1%

(Continues)

TABLE 1 | (Continued)

Identification			Correlation			Abundance in patterns (relative to max)				
UTG	Repr. species	Complex	Within complex	With others	Maximum abundance	A	B	C	D	E
19	Pre.nig	8	0.264	−0.006	2.59E-02	9.9%	20.6%	100.0%	76.9%	35.9%
36	All.tan	8	0.286	−0.001	1.28E-02	6.0%	22.5%	88.2%	99.8%	100.0%
47	Tre.med	8	0.253	0.017	9.93E-03	6.4%	38.4%	74.0%	42.0%	100.0%
62	Dia.pne	8	0.307	0.000	9.98E-03	6.2%	16.1%	100.0%	3.8%	57.9%
1	Fus.nuc.vin	9	0.229	−0.020	1.20E-01	25.6%	34.6%	100.0%	52.2%	87.5%
11	Bac.274	9	0.105	0.001	2.86E-02	9.8%	47.8%	87.1%	34.4%	100.0%
14	Fus.203	9	0.113	−0.013	3.04E-02	21.5%	38.6%	100.0%	2.6%	31.6%
73	Pre.ple	9	0.216	−0.013	6.41E-03	10.5%	14.7%	100.0%	1.2%	73.9%
89	Sac.957	9	0.058	0.011	3.26E-03	12.2%	100.0%	75.6%	0.0%	98.9%
7	Por.gin	10	0.292	−0.060	7.96E-02	0.0%	11.2%	20.2%	0.0%	100.0%
17	Por.end	10	0.317	−0.031	3.25E-02	6.2%	15.7%	58.4%	0.7%	100.0%
20	Cam.rec	10	0.332	−0.037	2.44E-02	12.0%	61.2%	39.2%	3.8%	100.0%
25	Tan.for	10	0.475	−0.070	2.87E-02	1.7%	8.7%	32.5%	2.0%	100.0%
28	Tre.den	10	0.498	−0.057	2.77E-02	0.9%	11.8%	25.5%	7.0%	100.0%

Note: Correlation of each UTG with the other UTGs was calculated using Pearson's *R* (as for Figure 2) and averaged within and outside its complex The maximum abundance of the UTG in a pattern is presented as the ratio to total UTG count ('Maximum Abundance' column), and the abundance in each pattern was then normalized by this maximum, yielding a relative abundance of 1 in the pattern where the UTG is more represented. A diverging green-to-red color palette is used to indicate values from minimum (green) to maximum (red) in the correlation and abundance columns. This table is an extract of Table S8, in which only 5 UTGs were kept by complex, according to their maximum abundance in a pattern, for readability concerns.

Pattern D). The mean boundary index for Complex 6 is intermediate, which is illustrated in Figure 4 by its wide interface with other complexes: 1, 2, 3, 4, 5 and 8.

4 | Discussion

The association between organisms within a niche is a foundational concept in ecology. Within the periodontal niche, these dynamic interactions are confined to microenvironments and are challenging to analyse in time and space. The composition and dynamics of microorganisms in periodontal sulci and pockets are influenced by various factors, including host genetics and lifestyle, which introduce variability. The interactions between microbes are multidimensional: our attempts to represent them in pauci-dimensional spaces limit the understanding by the human brain, as already discussed by Socransky and colleagues (Socransky et al. 1998). An inherent complexity of analyses from nucleic acid sequencing results from the impossibility to discriminate synonymous reads from different targets. In the present study, we tackled this issue by keeping all the relevant synonymous information from the assignation step, resulting in 79 UTGs (out of 394) that were not strictly monophyletic. This is important to consider when analysing the results, because they could be constituted from any of their identified components in different proportions and possibly varying between samples. As observed here, the corresponding taxa are in most of the cases closely related. However, our PRONEX assignment allowed us to keep apart synonymous taxa from the same FID at the lowest common taxonomic level, and thus to differentiate subspecies in

some cases. For instance, *F. nucleatum* was split into UTG001 (subspecies *vincentii* and *animalis*), UTG006 (subspecies *polymorphum*) and UTG093 (subspecies *nucleatum*). Using QIIME2 identification, some of the FIDs constituting these UTGs were assigned at the level of the *Fusobacterium* genus.

Variability, besides the methods, can also come from the studied population. In our case, we included patients from a single country, France, with a tight age range, employing strict inclusion and exclusion criteria as well as standardized sampling methodologies. Controlling this variability induces reduction of the representativity of the sample for the general population. Our recruitment strategy has thus excluded extreme forms of periodontitis, and young and old patients, in addition to the geographic restriction. Furthermore, the range of clinical measurements (e.g., pocket depth) was so limited that it impeded further correlations of our data with any parameters other than the health group itself. Some of the patterns detected here may be specific to the concerned population, and it is noticeable that *Schaalia odontolytica*, from Socransky's purple complex, is absent, while several other species are detected in various UTGs. Besides, *Aggregatibacter actinomycetemcomitans* (UTG324) is rare in our study, while it is not infrequent even in healthy sites from Moroccan periodontitis patients (Reddahi et al. 2023). Finally, the noticeable low abundance and frequency of Peptostreptococcaceae_[G-6] [Eubacterium]_*nodatum* (UTG183, formerly known as *Eubacterium nodatum*) contrast with previous findings (Haffajee et al. 2006), including Socransky's comment about its possible inclusion in the red complex (Socransky et al. 1998).

Besides these differences, our findings reaffirm the crucial role of red complex bacteria—*P. gingivalis*, *T. forsythia* and *T. denticola*—as biomarkers of periodontal disease (Socransky et al. 1998). Using high-resolution sequencing approach and advanced bioinformatics (PRONEX), we have added bacteria to this red complex, here Complex 10, namely 8 other *Treponema* UTGs, 3 *Prevotella* UTGs (in particular *Prevotella intermedia*, UTG056, Socransky's orange complex), 3 *Fretibacterium* UTGs, *P. endodontalis* (UTG017), *C. rectus* (UTG020, Socransky's orange complex) and 10 other UTGs. Besides this complex, with the strongest intra-complex associations, nine other complexes were identified, which also exhibited homogeneity. Thus, the observed alpha diversity increasing with disease severity may be due to the superposition of relatively homogeneous complexes rather than diversification over an original core. This complex ecological shift within the microbiota highlights a broader and more complex microbial landscape than previously recognized (Berezow and Darveau 2011).

Changes in microbe composition in a microenvironment are not perfectly linked to clinical diagnosis (Bonner et al. 2014): they may precede disease set-up (incubation) or clinical cure (microbial cure), or even reveal unexpected diversity that would be difficult to appreciate at the clinical level. Using another unsupervised method (k-means), we identified microbiota patterns based on patient samples, which correlated with clinical observations—although limited to the three health states, as previously discussed. However, these patterns are not perfectly defined by the exclusive protrusion of one particular complex, suggesting that species association involves intricate mechanisms beyond mere juxtaposition or superposition, including interactions such as adhesion and co-aggregation (Ochiai et al. 1993; Takemoto et al. 1995), or cooperations (Yost et al. 2017), leading to biofilm formation (Marsh and Bradshaw 1995). In our study, these ecological connectors that bridge microenvironments appear as 'boundary species' in our representations. UTGs from Complex 4 stand out with their high boundary indices (Table S8), especially the central and abundant *C. gracilis* (UTG008) in Figure 3, as well as those of Complexes 5 and 7, which are intermediaries between health and disease hemispheres. Complex 9 also exhibited high boundary indices but marked transitions within the disease-related complexes. The divergence observed between the results represented in Figure 3 and Table S8 is mainly due to the fact that the representation in Figure 3 of dyadic correlations undergo a threshold, unlike the indices of Table S8 that are threshold-less means. The difference between these two analyses may allow the appreciation of finer variations that are expected in a complex environment in which keystone pathogens—in low abundance but influential (Hajishengallis et al. 2012)—dwell together with accessory pathogens or co-pathogens (Zhou et al. 2021). These candidates can play a critical role in evolution towards disease and in provoking immune responses, further reshaping the microenvironment, and underline the need for other studies to evaluate the changes beyond microbe abundance.

Bacterial communities are not loose and planktonic but organized as three-dimensional biofilms with structures like corncob and hedgehog involving *Corynebacterium* filaments and bacteria from the *Lautropia*, *Streptococcus* or *Veillonella* genera (Mark Welch et al. 2016), which is consistent with Figure 4 and Complexes 6 and 2 composition, the latter having both low coefficient of variation between patterns and boundary index, thus exhibiting the characteristics of a ubiquitous core. These structures may include additional taxa, as suggested by our unbiased methodology and accurate taxonomic assignment, which future studies should confirm using specific probes.

The existence of various transitional states between health- and disease-associated communities implies multiple pathways of disease progression, which have significant clinical implications for early diagnosis and personalized treatment. The multiple branching between several distant UTGs or even complexes suggests that some microbial associations may compete or co-exist in parallel niches (Fukami 2010), indicating functional redundancy or complementarity that should be considered in therapeutic strategies.

Health and disease markers in Complexes 6 and 10, respectively, mark the extremities in our representations, suggesting a main axis and transitional states that challenge the distinction of gingivitis. This is supported by a linear relationship between gingivitis and periodontitis in terms of UTG abundance (Figure 3E,F). However, the microbiota patterns suggest that an A–C–E transition from health to periodontitis is consistent, as observed in both Figures 5 and 6, health being characterized by Complex 6 (and Complex 5), periodontitis by Complex 10 (and Complex 9) and gingivitis by an intermediate state. Pattern B would stand aside with the overabundance of Complexes 3 and 1, while Pattern D is characterized by the overabundance of Complex 7 and the strong repression of Complexes 1 and 10.

The strong repression of *P. gingivalis* and other members of Complex 10 in Pattern D (Tables S7 and S8) may represent a transitional state or a distinct type of periodontal disease, paralleling the bona fide periodontitis observed in Pattern E, reminding the 'Socransky' and 'Pg' traits linked to genetic specificities of the host (Offenbacher et al. 2016), respectively. Further analysis of these samples should provide insights into the entire microbiota, including non-bacterial microbes such as parasites (Martin-Garcia et al. 2022), archaea (de Cena et al. 2022), fungi (Karkowska-Kuleta et al. 2022), and viruses: herpesviruses (Jakovljevic et al. 2022), phages (Guo et al. 2024) and redondoviruses (Keeler et al. 2023; Makoa-Meng et al. 2023).

Future research should also push forward and evaluate the hypothesis of microbial complexes as metaorganisms (Bosch and McFall-Ngai 2011), where functional specialization might occur (Dragos et al. 2018) and could be paralleled to differentiation (Bell 1998). However, holobiont ecology should not be confined to this broad overview. It requires a deeper exploration of interactions between individual microbes and with their host to fully understand the complexities of these communities.

Finally, several limitations in our study should be acknowledged. First, our UTG identification methodology, while more precise than current methods, is probabilistic. Full-length 16S rRNA gene sequencing could improve precision (Buetas,

Jordán-López, López-Roldán, D'Auria, et al. 2024). Besides, our study does not address microbial communication (Mukherjee and Bassler 2019), 3D organization (Mark Welch et al. 2016), functional specialization (Yost et al. 2017; Yost et al. 2015; Sakanaka et al. 2022) or interactions with the host (Garcia-Arevalo et al. 2024). It is also worth mentioning that the 16S rRNA reads were not normalized to the number of copies in each genome: the results do not exactly reflect the number of bacteria in the samples.

As previously discussed, our patient recruitment might have impeded the representation of all forms of periodontal disease, as evidenced by the absence of *A. actinomycetemcomitans* (UTG324) from our interest taxa, while of major importance in some studies (Hbibi et al. 2022). This limits the exploration of periodontal infection diversity, particularly in mucositis, peri-implantitis and peri-implant healthy environments. Third, for reading purpose, we selected 162 UTGs based on their frequency in samples, but less abundant bacteria may still play a role as keystone pathogens: 49 of the unselected UTGs still reach at least 1% of reads in one or more samples (unpresented data). Fourth, the lack of patient follow-up in this study hinders the evaluation of microbial predisposition or early shifts in healthy patients that could lead to periodontal disease, echoing the long-term persistence of *A. actinomycetemcomitans* before symptom onset (Hbibi et al. 2022), that would validate the predictive value of microbial patterns on clinical parameters. Finally, significant progress remains to be made in characterizing the microbiota, as approximately 40% of the potentially represented taxa are uncultured phylotypes.

5 | Conclusion and Clinical Implications

Our study enriches Socransky's model by identifying 10 complexes instead of 5, by expanding the list of bacteria species belonging to the original red and green complexes, and by evidencing the existence of five general microbiota patterns in patients that characterize the transition from health to disease. Gingivitis appears as a transitional state, and Complex 10 dominates in periodontitis patients (Pattern E) but might not be the only type of diseased state, as evidenced by Pattern D. Because of its low frequency, Pattern D may represent a labile state, intermediate between Patterns C and E, or a different type of end-state that is poorly represented in our recruited samples and still to be characterized.

We identified boundary bacterial taxa bridging complexes that may play a key role in dysbiosis and should be investigated further. These ecological connectors could be targets for prophylactic measures, hampering the shift towards disease-associated complexes. Furthermore, the identification of specific bacterial taxa as reliable biomarkers for periodontal health (Complex 6) could help the development of efficient probiotics for guided colonization of disinfected pockets during periodontal therapy.

As already proposed elsewhere, the ratio between bacterial groups can serve as a diagnosis tool for dysbiosis (Meuric et al. 2017). The use of clustering to classify microbiota into patterns can improve these molecular biology strategies, paving the way for immediate scoring of microbiota pathogenicity from A (healthy) to D and E (very pathogenic levels). This advance in diagnosis could be used to assess the risk for future damage, but also to monitor treatment progression. This would complement the classical staging and grading system for periodontal disease classification (Tonetti et al. 2018) with an additional microbiological consideration, either as a third predictive/risk scale or as a component of the grading dimension as it may contribute to evaluate prognosis. The relevance of this indicator should be further validated in prospective cohorts.

Our study highlighted the abundance of *Treponema* genus UTGs in Complex 10, as well as the presence of other members only in complexes associated with disease: *T. socranskii* (UTG024, C7), *T. medium* (UTG047, C8) and *T.* sp. HMT 247 (UTG133, C9). Spirochaetes, in particular *T. denticola*, were the first bacteria identified as candidate aetiological agents of periodontitis, after the larger protozoa had been detected in periodontitis patients (reviewed in (Santi-Rocca 2022)). Their shape and characteristic motility, as well as these of the vibrio-like *C. rectus* (UTG020, C10), can be used for microscopic diagnosis of disease-linked patterns, in contrast to the sessile UTGs detected in Complex 6. Our analysis provides support to the usefulness of microscopy as an affordable and simple point-of-care tool to assess microbial risk in periodontal disease diagnosis and treatment follow-up, retaking with a long-term tradition (Listgarten 1976; Singletary et al. 1982) and echoing a more recent report (Bonner 2024).

Socransky and his colleagues forewarned about the limitations of their study, which they characterized as 'an initial attempt at evaluating inter-relationships among subgingival species' (Socransky et al. 1998). A quarter of century later, we have demonstrated the lasting relevance of this reference for the ecology of the periodontal microbiota in health and disease, and humbly contributed to complete it with novel taxa, complexes and health states.

Conflicts of Interest

The study has been funded by the Association Médicale contre les Infections Buccales and the Institut International de Parodontie,

which comprise clinicians that took part in the study. Julien Santi-Rocca and David F. Martín-García are part of Science and Healthcare for Oral Welfare, a private company that raises funds for research in science.

Data Availability Statement

The data that support the findings of this study are openly available in European Nucleotide Archive at https://www.ebi.ac.uk/ena/browser/home, reference number PRJEB83769.

References

Bell, G. 1998. "Model Metaorganism." *Science* 282, no. 5387: 248.

Berezow, A. B., and R. P. Darveau. 2011. "Microbial Shift and Periodontitis." *Periodontology 2000* 55, no. 1: 36–47.

Bonner, M. 2024. "Evaluation of Periodontitis Parameters and Plaque Examination by Microscopy: A Report on 20 Patients." *Frontiers in Dental Medicine* 5: 1451698.

Bonner, M., V. Amard, C. Bar-Pinatel, et al. 2014. "Detection of the Amoeba *Entamoeba gingivalis* in Periodontal Pockets." *Parasite* 21: 30.

Bosch, T. C., and M. J. McFall-Ngai. 2011. "Metaorganisms as the New Frontier." *Zoology (Jena, Germany)* 114, no. 4: 185–190.

Buetas, E., M. Jordán-López, A. López-Roldán, et al. 2024. "Full-Length 16S rRNA Gene Sequencing by PacBio Improves Taxonomic Resolution in Human Microbiome Samples." *BMC Genomics* 25, no. 1: 310.

de Cena, J. A., Y. Silvestre-Barbosa, A. Belmok, C. M. Stefani, C. M. Kyaw, and N. Damé-Teixeira. 2022. "Meta-Analyses on the Periodontal Archaeome." *Advances in Experimental Medicine and Biology* 1373: 69–93.

Dragos, A., H. Kiesewalter, M. Martin, et al. 2018. "Division of Labor During Biofilm Matrix Production." *Current Biology* 28, no. 12: 1903.e5–1913.e5.

Escapa, I. F., Y. Huang, T. Chen, et al. 2020. "Construction of Habitat-Specific Training Sets to Achieve Species-Level Assignment in 16S rRNA Gene Datasets." *Microbiome* 8, no. 1: 65.

Escapa, I. F., T. Chen, Y. Huang, P. Gajare, F. E. Dewhirst, and K. P. Lemon. 2018. "New Insights Into Human Nostril Microbiome From the Expanded Human Oral Microbiome Database (eHOMD): A Resource for the Microbiome of the Human Aerodigestive Tract." *mSystems* 3, no. 6: e00187-18.

Fong, S. B., E. Boyer, M. Bonnaure-Mallet, and V. Meuric. 2022. "Microbiota in Periodontitis: Advances in the Omic Era." *Advances in Experimental Medicine and Biology* 1373: 19–43.

Fukami, T. 2010. *Community Assembly Dynamics in Space*. Community ecology: Processes, models, and applications, 45–54.

Garcia-Arevalo, F., A. G. Leija-Montoya, J. González-Ramírez, et al. 2024. "Modulation of Myeloid-Derived Suppressor Cell Functions by Oral Inflammatory Diseases and Important Oral Pathogens." *Frontiers in Immunology* 15: 1349067.

Guo, X., X. Wang, J. Shi, et al. 2024. "A Review and New Perspective on Oral Bacteriophages: Manifestations in the Ecology of Oral Diseases." *Journal of Oral Microbiology* 16, no. 1: 2344272.

Haffajee, A. D., R. P. Teles, and S. S. Socransky. 2006. "Association of *Eubacterium nodatum* and *Treponema denticola* With Human Periodontitis Lesions." *Oral Microbiology and Immunology* 21, no. 5: 269–282.

Hajishengallis, G., R. P. Darveau, and M. A. Curtis. 2012. "The Keystone-Pathogen Hypothesis." *Nature Reviews Microbiology* 10, no. 10: 717–725.

Hbibi, A., A. Bouziane, B. Lyoussi, M. Zouhdi, and D. Benazza. 2022. "*Aggregatibacter actinomycetemcomitans*: From Basic to Advanced Research." *Advances in Experimental Medicine and Biology* 1373: 45–67.

Jakovljevic, A., M. Andric, J. Jacimovic, J. Milasin, and J. E. Botero. 2022. "Herpesviruses in Periodontitis: An Umbrella Review." *Advances in Experimental Medicine and Biology* 1373: 139–155.

Jiao, J., M. Bie, X. Xu, et al. 2022. "*Entamoeba gingivalis* Is Associated With Periodontal Conditions in Chinese Young Patients: A Cross-Sectional Study." *Frontiers in Cellular and Infection Microbiology* 12: 1020730.

Karkowska-Kuleta, J., D. Satala, M. Smolarz, M. Zawrotniak, and M. Rapala-Kozik. 2022. "Fungi-A Component of the Oral Microbiome Involved in Periodontal Diseases." *Advances in Experimental Medicine and Biology* 1373: 113–138.

Keeler, E. L., C. Merenstein, S. Reddy, et al. 2023. "Widespread, Human-Associated Redondoviruses Infect the Commensal Protozoan *Entamoeba gingivalis*." *Cell Host & Microbe* 31, no. 1: 58.e5–68.e5.

Klindworth, A., E. Pruesse, T. Schweer, et al. 2013. "Evaluation of General 16S Ribosomal RNA Gene PCR Primers for Classical and Next-Generation Sequencing-Based Diversity Studies." *Nucleic Acids Research* 41, no. 1: e1.

Listgarten, M. A. 1976. "Structure of the Microbial Flora Associated With Periodontal Health and Disease in Man: A Light and Electron Microscopic Study." *Journal of Periodontology* 47, no. 1: 1–18.

Makoa-Meng, M., R. Semmar, A. Antezack, et al. 2023. "Correlation of Redondovirus and *Entamoeba gingivalis* Detections in the Human Oral Cavity Suggests That This Amoeba Is Possibly the Redondovirus Host." *International Journal of Molecular Sciences* 24, no. 7: 6303.

Mark Welch, J. L., B. J. Rossetti, C. W. Rieken, F. E. Dewhirst, and G. G. Borisy. 2016. "Biogeography of a Human Oral Microbiome at the Micron Scale." *Proceedings of the National Academy of Sciences of the United States of America* 113, no. 6: E791–E800.

Marsh, P. D., and D. J. Bradshaw. 1995. "Dental Plaque as a Biofilm." *Journal of Industrial Microbiology & Biotechnology* 15, no. 3: 169–175.

Martin-Garcia, D. F., M. Sallam, G. Garcia, and J. Santi-Rocca. 2022. "Parasites in Periodontal Health and Disease: A Systematic Review and Meta-Analysis." *Advances in Experimental Medicine and Biology* 1373: 95–111.

Meuric, V., S. le Gall-David, E. Boyer, et al. 2017. "Signature of Microbial Dysbiosis in Periodontitis." *Applied and Environmental Microbiology* 83, no. 14: e00462-17.

Mukherjee, S., and B. L. Bassler. 2019. "Bacterial Quorum Sensing in Complex and Dynamically Changing Environments." *Nature Reviews Microbiology* 17, no. 6: 371–382.

Ochiai, K., T. Kurita-Ochiai, Y. Kamino, and T. Ikeda. 1993. "Effect of Co-Aggregation on the Pathogenicity of Oral Bacteria." *Journal of Medical Microbiology* 39, no. 3: 183–190.

Offenbacher, S., K. Divaris, S. P. Barros, et al. 2016. "Genome-Wide Association Study of Biologically Informed Periodontal Complex Traits Offers Novel Insights Into the Genetic Basis of Periodontal Disease." *Human Molecular Genetics* 25, no. 10: 2113–2129.

Reddahi, S., A. Bouziane, K. Dib, H. Tligui, and O. Ennibi. 2023. "qPCR Detection and Quantification of *Aggregatibacter actinomycetemcomitans* and Other Periodontal Pathogens in Saliva and Gingival Crevicular Fluid Among Periodontitis Patients." *Pathogens* 12, no. 1: 76.

Sakanaka, A., M. Kuboniwa, S. Shimma, et al. 2022. "*Fusobacterium nucleatum* Metabolically Integrates Commensals and Pathogens in Oral Biofilms." *mSystems* 7, no. 4: e0017022.

Santi-Rocca, J. 2022. "Advances in Experimental Research About Periodontitis: Lessons From the Past, Ideas for the Future." *Advances in Experimental Medicine and Biology* 1373: 1–15.

Singletary, M. M., J. J. Crawford, and D. M. Simpson. 1982. "Dark-Field Microscopic Monitoring of Subgingival Bacteria During Periodontal Therapy." *Journal of Periodontology* 53, no. 11: 671–681.

Socransky, S. S., A. D. Haffajee, M. A. Cugini, C. Smith, and R. L. Kent Jr. 1998. "Microbial Complexes in Subgingival Plaque." *Journal of Clinical Periodontology* 25, no. 2: 134–144.

Takemoto, T., T. Hino, M. Yoshida, K. Nakanishi, M. Shirakawa, and H. Okamoto. 1995. "Characteristics of Multimodal Co-Aggregation Between *Fusobacterium nucleatum* and Streptococci." *Journal of Periodontal Research* 30, no. 4: 252–257.

Tonetti, M. S., H. Greenwell, and K. S. Kornman. 2018. "Staging and Grading of Periodontitis: Framework and Proposal of a New Classification and Case Definition." *Journal of Clinical Periodontology* 45, no. S20: S149–S161.

Yost, S., A. E. Duran-Pinedo, K. Krishnan, and J. Frias-Lopez. 2017. "Potassium Is a Key Signal in Host-Microbiome Dysbiosis in Periodontitis." *PLoS Pathogens* 13, no. 6: e1006457.

Yost, S., A. E. Duran-Pinedo, R. Teles, et al. 2015. "Functional Signatures of Oral Dysbiosis During Periodontitis Progression Revealed by Microbial Metatranscriptome Analysis." *Genome Medicine* 7, no. 1: 27.

Zhou, P., D. Manoil, G. N. Belibasakis, and G. A. Kotsakis. 2021. "Veillonellae: Beyond Bridging Species in Oral Biofilm Ecology." *Frontiers in Oral Health* 2: 774115.

Supporting Information

Additional supporting information can be found online in the Supporting Information section.